JGR Atmospheres

RESEARCH ARTICLE
10.1029/2018JD029064

On the Interpretation of the ENSO Signal Embedded in the Stable Isotopic Composition of Quelccaya Ice Cap, Peru

J. V. Hurley[1,2], Mathias Vuille[2], and Douglas R. Hardy[3]

[1]College of Earth, Ocean and Atmospheric Sciences, Oregon State University, Corvallis, OR, USA, [2]Department of Atmospheric and Environmental Sciences, University at Albany, Albany, NY, USA, [3]Department of Geosciences, University of Massachusetts, Amherst, MA, USA

Key Points:
- ENSO influences delta(superscript 18)O on Quelccaya by modulating upstream monsoon activity, affecting water vapor delta values over the western Amazon basin
- The influence of ENSO-induced regional temperature variability alone is opposite the observed Quelccaya delta (superscript 18)O response to ENSO
- ENSO-related changes to Quelccaya snow gain/loss are insufficient to account for the observed response of Quelccaya delta (superscript 18)O to ENSO

Supporting Information:
- Supporting Information S1
- Data Set S1
- Data Set S2
- Data Set S3

Correspondence to:
J. V. Hurley,
jvhurley12@gmail.com

Citation:
Hurley, J. V., Vuille, M., & Hardy, D. R. (2019). On the interpretation of the ENSO signal embedded in the stable isotopic composition of Quelccaya Ice Cap, Peru. *Journal Geophysical Researcher: Atmospheres*, *124*, 131–145. https://doi.org/10.1029/2018JD029064

Received 25 MAY 2018
Accepted 17 DEC 2018
Accepted article online 21 DEC 2018
Published online 7 JAN 2019

Abstract The $\delta^{18}O$ signal in ice cores from the Quelccaya Ice Cap (QIC), Peru, corresponds with and has been used to reconstruct Niño region sea surface temperatures (SSTs), but the physical mechanisms that tie El Niño–Southern Oscillation (ENSO)-related equatorial Pacific SSTs to snow $\delta^{18}O$ at 5,680 m in the Andes have not been fully established. We use a proxy system model to simulate how QIC snow $\delta^{18}O$ varies by ENSO phase. The model accurately simulates higher and lower $\delta^{18}O$ values during El Niño and La Niña, respectively. We then explore the relative roles of ENSO forcing on different components of the forward model: (i) the seasonality and amount of snow gain and loss at the QIC, (ii) the initial water vapor $\delta^{18}O$ values, and (iii) regional temperature. Most (more than two thirds) of the ENSO-related variability in the QIC $\delta^{18}O$ can be accounted for by ENSO's influence on South American summer monsoon (SASM) activity and the resulting change in the initial water vapor isotopic composition. The initial water vapor $\delta^{18}O$ values are affected by the strength of upstream convection associated with the SASM. Since convection over the Amazon is enhanced during La Niña, the water vapor over the western Amazon Basin—which serves as moisture source for snowfall on QIC—is characterized by more negative $\delta^{18}O$ values. In the forward model, higher initial water vapor δ-values during El Niño yield higher snow $\delta^{18}O$ at the QIC. Our results clarify that the ENSO-related isotope signal on Quelccaya should not be interpreted as a simple temperature response.

Plain Language Summary The Quelccaya Ice Cap in the Andes Mountains of Peru is retreating because of global warming, and ice cores from Quelccaya are some of the best records that we have for climate from the last 2,000 years. Quelccaya is the world's largest tropical ice cap, and as such it is an important regional water resource. The climate record from Quelccaya's ice core chemistry has long been tied to El Niño activity. However, it is not obvious how ocean water temperature in the equatorial Pacific alters the chemistry of snow that falls at 5,680 m above sea level in the Andes Mountains. We used 15 years of weather station data from the summit of Quelccaya, along with a climate model, to show that it is the intensity of rainfall over the Amazon rainforest that changes the chemistry of snow at Quelccaya. For example, the rainfall over the Amazon is more intense during La Niña, causing the water vapor over the western Amazon to be lighter. This lighter version of water vapor is then transported up to the height of Quelccaya and makes snow with a lower chemical signature.

1. Introduction

The 2015–2016 El Niño ranks as one the highest-amplitude El Niño–Southern Oscillation (ENSO) events observed since 1950 (L'Heureux et al., 2017). Equatorial Pacific sea surface temperature (SST) anomalies for 2015–2016 were at least as large as they were during the historically important 1972–1973, 1982–1983, and 1997–1998 events. December-January-February (DJF) Niño SST regions 3.4 and 4 SST anomalies were at record values: Niño region 4 SST DJF anomalies were nearly 1.5°K, compared with 0.5°–0.7°K for the three above mentioned extreme historic events. This was the first extreme El Niño event of the 21st century, and a consequence of both prevailing 2014 warmth and long-term global warming (Santoso et al., 2017).

The 2015–2016 El Niño had profound impacts around the globe. For instance, the boreal winter was one of the most intense coastal erosion seasons recorded in the western United States over the past 145 years

(Barnard et al., 2017). A record-breaking cholera epidemic occurred in East Africa, the worst such event since the last major El Niño in 1997–1998. Closer to the tropical Pacific, record-breaking warmth and persistent drought conditions were recorded in parts of the Amazon rainforest during the 2015–2016 El Niño (Jiménez-Muñoz et al., 2016). In the tropical Andes, glaciers have historically also been affected by strong ENSO events, with large negative mass balance and ice wastage during El Niño events (Francou et al., 2003; Francou et al., 2004; Rabatel et al., 2013; Vuille et al., 2008).

We have been continuously monitoring temperature, snow height change, and other meteorological variables for the past 14 years at the summit of the Quelccaya Ice Cap (QIC) in Peru with an Automated Weather Station (AWS, 13.93°S, 70.82°W). Temperature at Quelccaya is commonly higher during El Niño, and monthly temperature anomalies at Quelccaya during the 2015–2016 El Niño were as much as 2 standard deviations (σ) above average (Figure 1a). For the first time since monitoring began in 2003, there was an annual net decrease in Quelccaya surface snow height (−0.04 m) for the hydrologic year of June 2015 through May 2016 (Figures 1b–1c). This contrasts with the mean annual net snow height gain of about 1.8–2.0 m.

As with snow height, water stable isotope ratios (oxygen-^{18}O and ^{16}O; hydrogen ^{2}H, or deuterium [D], and ^{1}H) recorded in snow and ice at Quelccaya are also sensitive to ENSO forcing (Thompson et al., 2013, 2017). Interannual variability of stable isotope ratios from Quelccaya snow and ice has been linked to tropical Pacific SSTs and ENSO. However, the physical processes that account for this relationship have not been fully explained.

To do this, we identify and test the sensitivity of stable isotope concentrations to physical mechanisms that are tied to or forced by ENSO. By understanding these linkages, we can inform our interpretation of climate change (Bradley et al., 2003, 2004, 2009) at Quelccaya and across the broader tropical Andean region. ENSO variability of stable isotope ratios, congruent with those from Quelccaya, have been observed at other Andean and Amazon locations (Vuille et al., 2003b; Vimeux et al., 2009). These include ice core locations at Huascarán in Peru and Sajama in Bolivia, as well as Global Network for Isotopes in Precipitation sites throughout the region (Vuille & Werner, 2005). Evidence has long pointed toward a relationship between ENSO, Amazon convection and the hydrologic stable isotope values (Vuille et al., 2003a). We expect that our results presented here are relevant for deciphering stable isotope records that are sensitive to upstream convection, which is in turn driven by higher-order forcings such as tropical SSTs or the large-scale circulation.

In addition to the AWS monitoring at Quelccaya, snow layer δ^{18}O has been measured in samples collected from annual snow pits completed at the summit of the ice cap (Figure 1d). When we sort the snow δ^{18}O values by ENSO phase based on the Oceanic Niño Index (ONI; Climate Prediction Center, 2018; Figure 2), The δ^{18}O is significantly higher during El Niño (about −17‰) compared with La Niña (about −22‰), in ways that are consistent with Thompson et al.'s (2013) linear model for tropical Pacific SST reconstruction based on Quelccaya δ^{18}O. For reference, the average δ^{18}O from the 2015–2016 snow pit was about −15‰.

There is a close positive association between temperature on Quelccaya and tropical Pacific SST (Figure 1a). The warmer the Pacific, the more positive the temperature anomalies at QIC, indicated by the gradual transition from cold (blue) to warm (red) SST anomalies' in Figure 1a showing temperature anomalies at QIC increasing from left to right. The 2015–2016 El Niño stands out as an extreme anomaly, with 8 out of the 10 anomalously warmest months at QIC occurring during this event. The exceptional nature of this event is also highlighted by temperature at QIC exceeding +1.5 σ for a period of 6 months; the probability of an event exceeding +1.5 sigma in a normally distributed data set corresponds to $p < 0.07$. There is a similar, albeit weaker, control of tropical Pacific SST on accumulation rates at QIC (Figure 1b), with colder and warmer SSTs corresponding, respectively, with generally higher and lower snowfall totals.

For reference and context we compare the in situ observations from the summit of Quelccaya (Figure 1) with ENSO influence on regional climate variability (Figure 3). The hydrologic cycle is more active with enhanced austral summer precipitation during La Niña over the Amazon Basin (Figures 3a and 3b), particularly over the central Amazon Basin. Patterns for ENSO variability over the tropical Andes are characterized by discrete areas with enhanced precipitation during El Niño, including over Quelccaya. This contrasts the reverse pattern that we observe from AWS measurements (Figures 1c and 1d) and highlights the usefulness of the continuous AWS measurements in this remote Alpine environment. South of the Amazon Basin, precipitation is greater during El Niño over much of southeastern South America. Temperatures over tropical

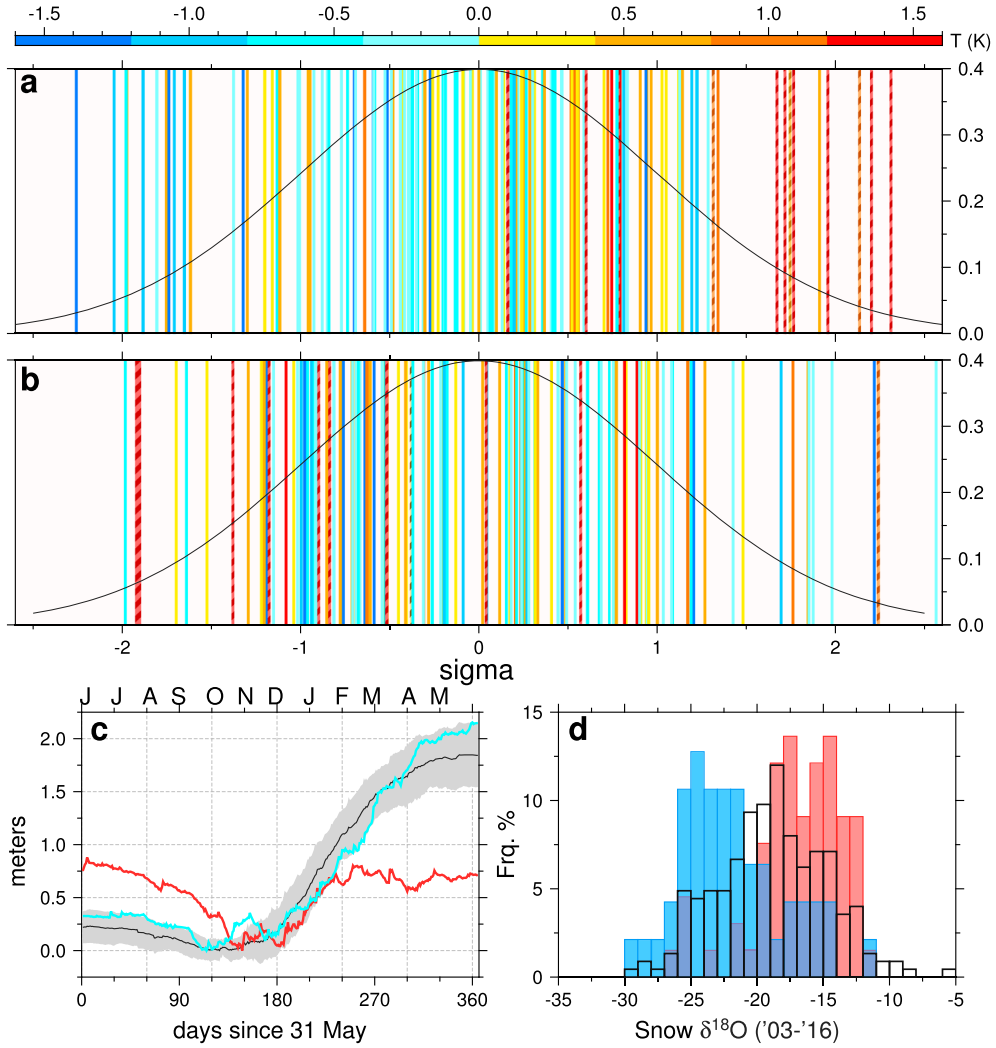

Figure 1. (a) Distribution of monthly Quelccaya Automated Weather Station temperature anomalies expressed as departures in standard deviations from the monthly mean values (2003–2017). Vertical lines are colored according to the concurrent monthly Oceanic Nino Index sea surface temperature anomaly (see temperature scale on top). Dashed lines correspond to the 2015–2016 El Niño–Southern Oscillation event. (b) As in (a) but for net monthly snow height change values. Normal distribution in (a) and (b) are plotted as gray curves with probability plotted on *y* axis. (c) Hydrologic year (June-May) cumulative snow height change at Quelccaya, referenced to the yearly minimum cumulative snow height (0 on the *y* axis). The solid black curve is the multiyear mean (2003–2017), and the gray shading is the mean ±1 standard deviation. The red curve indicates the 2015–2016 El Niño event, while the cyan curve depicts the 2016–2017 La Niña. *X* axis indicates day in the hydrologic year or days since 31 May; 1 June = day 1. (d) Observed monthly averaged $\delta^{18}O$ frequency distribution between 2003 and 2016 from snow samples (black outline bars = all data, red = El Niño, and blue = La Niña). Purple bars reflect intersection of red (El Niño) and blue (La Niña) distributions.

and subtropical South America are warmer during El Niño (Figures 3c and 3d), consistent with AWS observations from Quelccaya (Figure 1a). ENSO variability of lower troposphere (850 hPa) circulation patterns is characterized by enhanced easterly flow over the Amazon Basin during El Niño, and during La Niña there is statistically signifcant reduction in the strength of the northerly low-level jet (Figure 3d). Though the statistical significance of these differences are limited by the short time period considered (2003–2017), the broad climate patterns in Figure 3 are consistent with previous investigation of ENSO variability of South American climate (Krishnamurthy & Misra, 2010; Vuille & Werner, 2005).

To explore the physical processes that connect tropical Pacific SSTs to Quelccaya $\delta^{18}O$ on interannual time scales, we here use a proxy system model (PSM) that we recently developed for simulating stable oxygen and hydrogen isotope ratios in tropical Andean ice cores (Hurley et al., 2016). We complete a series of simulations

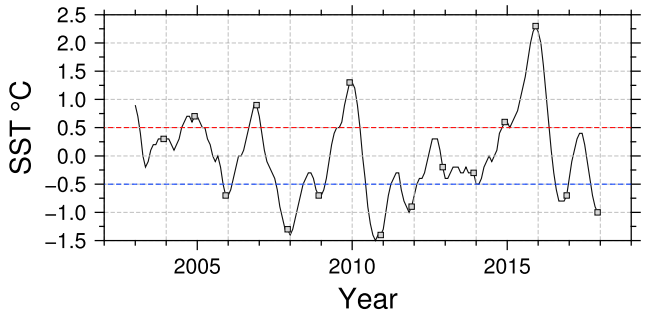

Figure 2. Oceanic Niño Index time series of sea surface temperature anomalies. December-January-February seasons are indicated by small gray squares, and red and blue horizontal dashed lines indicate the 0.5 °C threshold to characterize seasons as El Niño and La Niña.

that probe the sensitivity of the isotopic composition in Andean snowfall in response to warm and cold ENSO phases. We quantify the role played by ENSO in changing the isotopic composition of Andean snowfall by modulating (i) the local snow gain/loss at Quelccaya, (ii) regional air temperature (and its influence on humidity) around Quelccaya, and (iii) water vapor isotope ratios over the western Amazon Basin, one factor at a time. This approach is designed to answer the question whether ENSO influences the stable isotopic composition of snowfall on Quelccaya $\delta^{18}O$ principally by means of the local snow gain/loss, air temperature, or the large-scale circulation upstream over the South American summer monsoon (SASM) domain.

Our results show that Quelccaya $\delta^{18}O$ interannual variability is most sensitive to the lower troposphere water vapor $\delta^{18}O$ composition over the

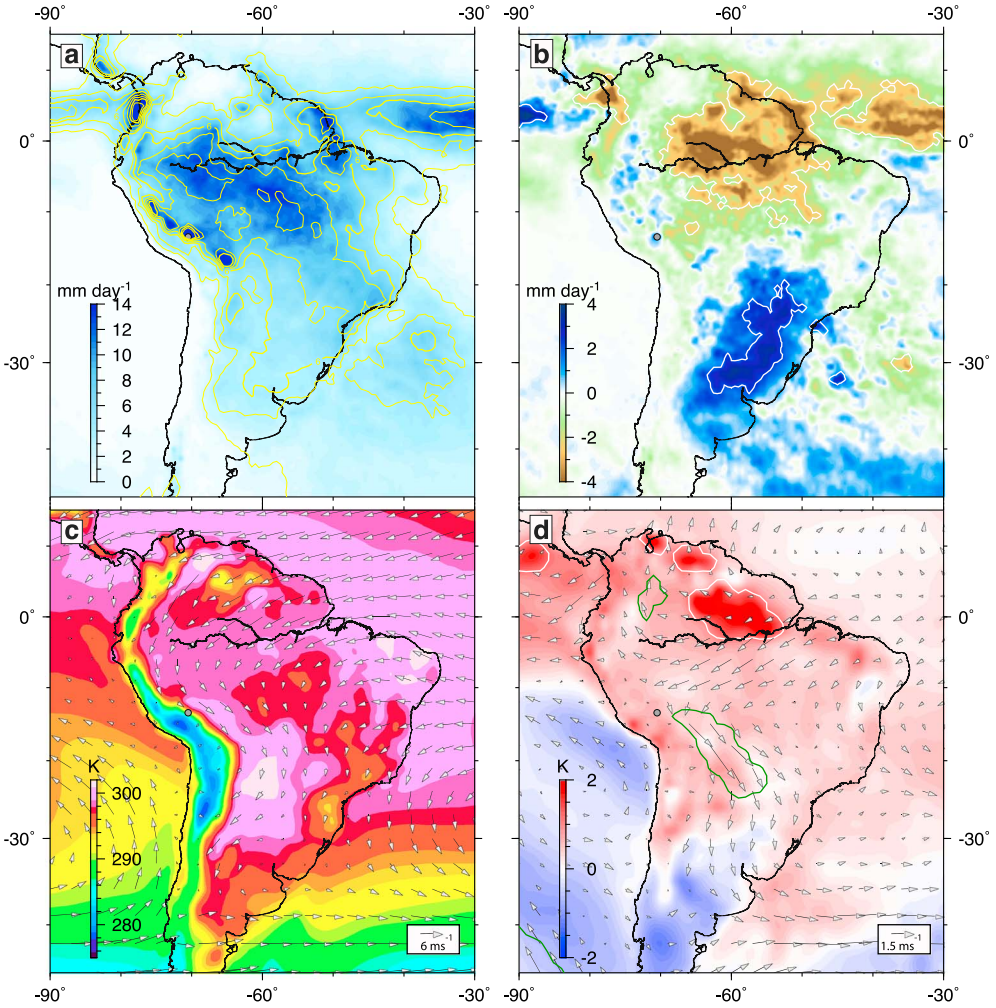

Figure 3. (a) DJF mean precipitation from the NASA Tropical Rainfall Measuring Mission 3B42 product for La Niña (shaded) and El Niño (contours, interval = 2 mm/day). (b) ENSO variability (El Niño minus La Niña, shaded) for mean DJF TRMM precipitation. (c) La Niña mean DJF surface temperature (shaded) and lower troposphere (850 hPa) horizontal winds (vectors). (d) ENSO variability (El Niño minus La Niña) of surface temperature (shaded) mean DJF and lower troposphere horizontal winds (vectors). Values in (c) and (d) were calculated from the ERA-Interim realysis, and scale vectors are provided for reference. Location of Quelccaya Ice Cap is indicated by the small gray circle. Areas where the ENSO variability is statistically significant at the 95% confidence level (*t* test) are surrounded by contours in (b) for precipitation (white contour) and in (d) for both surface temperature (white contour) and horizontal wind (green contour). DJF = December-January-February; ENSO = El Niño–Southern Oscillation.

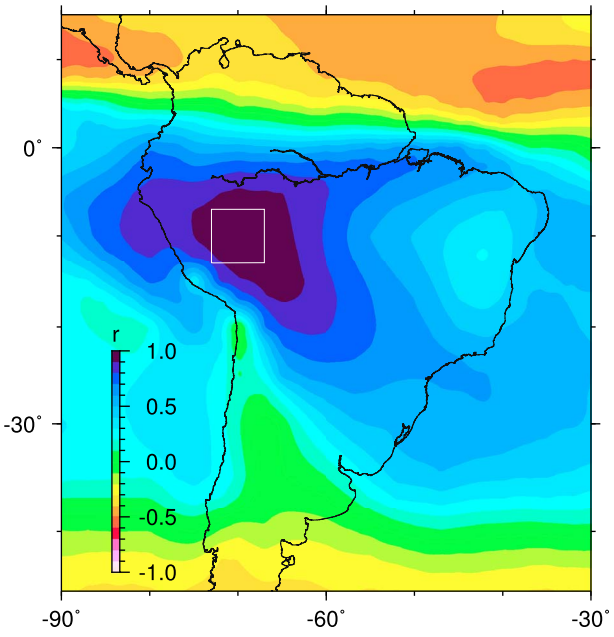

Figure 4. Correlation coefficients (r) for time series of lower troposphere (850 hPa) water vapor isotope ratios (IsoGSM) averaged over the western Amazon Basin (white box) versus water vapor isotope ratios at each grid cell.

western Amazon Basin, which in turn is reflecting upstream and SASM activity (Grootes et al., 1989; Hurley et al., 2015; Samuels-Crow et al., 2014). In the PSM, the lower troposphere water vapor isotope ratio over the western Amazon Basin functions as the initial water vapor δ^{18}O value, or the initial isotope ratio of the vapor that subsequently undergoes convection, condensation, and fractionation up to the altitude of Quelccaya. Regional temperature variability or ENSO-induced changes in the local snow gain/loss (timing and amount of snowfall on QIC) on the other hand, are of minor relevance. This result provides a physical mechanism connecting the 1800-year Quelccaya δ^{18}O archive to both tropical Pacific SST and the past history of the SASM. Data and methods are discussed in the following section, including an overview of the ENSO sensitivity test performed with our PSM model. Results of the PSM simulations are presented in section 3. We present a discussion of the significance and limitations of the simulation results, as well as a brief set of conclusions in the final section 4.

2. Model, Data, and Approach

2.1. Proxy System Model

We explore the influence of ENSO on several climate parameters, which in turn serve as forcing terms of Quelccaya δ^{18}O in our PSM model. We complete a series of sensitivity tests using the PSM that was developed and presented with a more detailed explanation in Hurley et al. (2016). The PSM describes the mechanistic and forward processes (Evans et al., 2013) that record Andean ice δ^{18}O. The model simulates annual snow layer δ^{18}O profiles by solving for daily changes in the snow isotope ratio at the summit of Quelccaya as a function of (i) the local snow gain/loss, (ii) temperature, and (iii) the isotope ratio of the initial water vapor, defined here as the lower troposphere water vapor δ value over the western Amazon Basin.

The local snow gain/loss, taken as the AWS measurements of snow height change (Δh_s), determines model daily changes in thickness of the snow profile. When the daily snow accumulation is positive, a fresh snow layer is added to the profile with a δ^{18}O value modeled as a product of Rayleigh fractionation during transport from the lower troposphere (850 hPa) over the western Amazon Basin, up to an altitude above the Quelccaya summit (400 hPa). We define here the western Amazon Basin for temperature and isotope ratio composite calculations as the area from 67°W–73°W and 7°S–13°S. Lower troposphere water vapor isotope ratios from grid cells in this area share a common variability (Figure 4), which supports the definition and selection of this area. On days of negative snow height change, the snow profile is reduced, by removing snow from the surface, and the δ^{18}O of the new snow surface is modeled, with isotopic enrichment occurring as a function of the sublimation rate (Hurley et al., 2016).

Air temperature (T) impacts the model scheme as vertical profiles from the lower to the upper troposphere are used to characterize the Rayleigh fractionation models. Fractionation factors and humidity, q, are temperature dependent, and therefore, the seasonality of isotopic fractionation partly reflects the seasonal cycle of temperature.

The isotope ratio of the initial water vapor ($\delta_{v,i}$) also serves as input for the Rayleigh fractionation model. Here we use the water vapor isotopic composition of the lower troposphere over the western Amazon Basin. The seasonal and interannual changes of this water vapor δ value reflect the degree of rainout occurring as a result of upstream convection over the Amazon Basin.

2.2. Data

Monthly temperature data and daily snow height change data from the AWS on the summit of QIC were used in this study (see supporting information, SI). The sensitivity of monthly temperature anomalies to ENSO conditions in the tropical Pacific is illustrated in Figure 1. Daily snow height change is used as a proxy for snowfall and sublimation. Snow δ^{18}O data from snow pit sampling over the past decade are also summarized in Figure 1 (provided in the SI) to illustrate the ENSO impact on the snow isotopic composition

Table 1
Model Parameter 850 hPa Initial Values for the Control Simulations

Parameter	Q-CTRL	El-CTRL	La-CTRL
q_i (kg/kg)	0.0140	0.0141	0.0137
δD_i (‰)	−128	−119	−138
T_i (°C)	15.6	16.4	15.4

Note. Example values listed here for reference are for 1 January.

at Quelccaya. A more detailed explanation of the AWS, data collection, and snow sampling was presented in Hurley et al. (2015).

Rayleigh fractionation models were calculated on a daily time step using western Amazon Basin information on water vapor and temperature from the reanalysis data, and water vapor isotopologue satellite observations, all averaged over the western Amazon Basin to the east of QIC (67°W–73°W, 7°S–13°S). For reanalysis, we use 6-hourly pressure level output from the European Centre for Medium-Range Weather Forecasts ERA-Interim product (Dee et al., 2011). For satellite information on water vapor isotopologue concentrations, we use observations from the National Aeronautics and Space Administration (NASA) Tropsphere Emission Spectrometer (TES). We use the bias-corrected level 2 version 6 Lite Product with the averaging kernels for HDO and H_2O products (L2v005litev08; National Aeronautics and Space Administration, 2015; Worden et al., 2011, 2012). The mean seasonal cycle of water vapor isotope ratios was calculated from TES observations. Because the remotely sensed TES observations are spatially and temporally discontinuous, the ENSO-phase variability was calculated separately from the historical period using the isotope reanalysis product, IsoGSM (Yoshimura et al., 2008), for the lower troposphere (850 hPa). Oxygen isotope ratios are not measured by TES, therefore Rayleigh model initial vapor oxygen isotope ratios were approximated from hydrogen isotope ratios using the linear empirical relationship of the Global Meteoric Water Line (Craig, 1961).

Warm and cold ENSO-phase episodes are considered based on the ONI, version 5 (Figure 2), which is a 3-month running average of ERSST.v4 SST anomalies in the Niño 3.4 region (5°S–5°N, 120°W–170°W) (Huang et al., 2015). Warm and cold ENSO-phase months (El Niño and La Niña, respectively) are defined by the ONI as those where the 3-month running mean SST anomaly for that month exceeds 0.5°C for a minimum of five overlapping 3-month-average seasons (Climate Prediction Center, 2018).

To complement the results of our simulations, we computed field correlation and regression coefficients between observed and simulated Quelccaya $\delta^{18}O$ and both SSTs and outgoing longwave radiation (OLR). These analyses are intented to test the sensitivity of Quelccaya $\delta^{18}O$ to spatial patterns of both ENSO (SSTs) and the SASM-related convection (OLR). For SSTs we use the Extended Reconstructed Sea Surface Temperature Version 5 (ERSSTv5; Huang et al., 2017). For OLR we use the 1° by 1° daily Interpolated OLR product from the National Oceanic and Atmospheric Administration (Lee, 2014).

2.3. Approach: ENSO-Phase Composites

2.3.1. Control Simulations

We first present our three control (CTRL) simulations; the mean Quelccaya CTRL simulation (Q-CTRL), an El Niño CTRL simulation (El-CTRL), and a La Niña CTRL simulation (La-CTRL). The mean control simulation, Q-CTRL, is a PSM simulation using the full record of snow height change from Quelccaya and ERA-Interim air temperature profiles for that same period (2003–2017). At the time this manuscript was prepared, snow height change data from Quelccaya were available through May 2017. The configuration of the Q-CTRL simulation is the same as the CTRL simulation presented in Hurley et al. (2016), wherein it was demonstrated that the model is capable of simulating the observed mean and seasonal cycle of Quelccaya $\delta^{18}O$. For the ENSO-phase CTRL simulations (El-CTRL and La-CTRL), we subsample the record of AWS snow height, reanalysis temperature, and both TES and IsoGSM initial vapor δ-values to only include periods that are characterized by ENSO conditions. ENSO-phase composites of Quelccaya AWS snow height, ERA-Interim temperature, and initial water vapor δ values are calculated as anomalies from the climatology. Rayleigh model initial vapor conditions for humidity, temperature, and isotope ratio for the control simulations are reported in Table 1. The distribution of Quelccaya snow $\delta^{18}O$ values from the control simulations (Q-CTRL, El-CTRL, and La-CTRL; Figure 5) resemble the observed distribution of values (Figure 1d). The

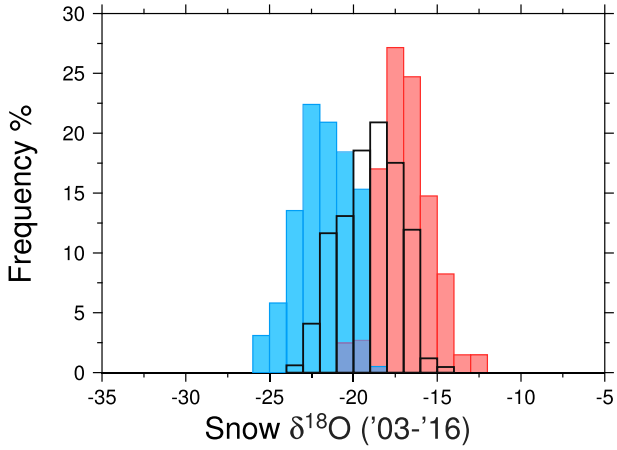

Figure 5. Frequency percent distribution of Quelccaya snow $\delta^{18}O$ in the control simulation, stratified by El Niño–Southern Oscillation phase. Black outline bars = Q-CTRL, red = El-CTRL, and blue = La-CTRL. Purple bars reflect intersection of red (El-CTRL) and blue (La-CTRL) distributions.

mean conditions are appropriately simulated, but the observed variability is underestimated. The El-CTRL and La-CTRL PSM simulations, which are driven by the observed composite ENSO variability, are capable of reproducing the observed ENSO variability of Quelccaya snow $\delta^{18}O$. As with the Q-CTRL simulation, the distribution of simulated values for each ENSO phase underestimates the observed variability. This is likely due to the absence of synoptic-scale temperature variability in these simulations. In a previous study (Hurley et al., 2016), we accounted for synoptic-scale variability via incorporation of South American cold air incursions in the PSM and found this necessary to account for the observed intraseasonal variability. Here in this study, we focus on the ENSO variability of Quelccaya $\delta^{18}O$ and so we use the simple control configuration of the PSM without synoptic-scale variability. We next explore the influence of the three primary model components (local snow gain/loss, Δh_s, temperature, T, and initial water vapor δ value, $\delta_{v,i}$), their ENSO-related variability, and their relative roles in forcing Quelccaya $\delta^{18}O$.

2.3.2. ENSO-Phase Simulations

For each of the three climate variables (model components) considered in this study, both a warm (El Niño) and a cold (La Niña) phase simulation were completed. Therefore, beyond the three control simulations, we completed six additional ENSO-phase simulations. The ENSO-phase simulations have the same configuration as Q-CTRL, except one parameter was varied at a time, consistent with the observed ENSO-phase composite time evolution of that parameter. The ENSO-phase simulations are summarized as follows: (1) an El Niño local snow gain/loss simulation based on the Q-CTRL configuration with only the local snow gain/loss (El-Δh_s) allowed to vary, (2) a La Niña local snow gain/loss simulation (La-Δh_s), (3) an El Niño temperature simulation (El-T), (4) a La Niña temperature simulation (La-T), (5) an El Niño initial water vapor δ-value simulation (El-$\delta_{v,i}$), and finally (6) a La Niña initial water vapor δ value simulation (La-$\delta_{v,i}$). These ENSO-phase simulations were forced based on observed ENSO-phase composites of the local snow gain/loss, temperature, and initial water vapor isotope ratios. We note here that the El-T and La-T simulations were forced with ENSO-phase temperature variability and as a consequence of temperature the water vapor concentration also varies as a response of the model in these simulations.

2.3.3. Local Snow Gain/Loss

Information on the local snow gain/loss cycle is from AWS observations at the summit of Quelccaya. What we describe here as the local snow gain/loss refers to the precipitation and sublimation of snow at the summit of Quelccaya (Figure 6). The seasonality of these processes are sensitive to ENSO phase, which yields snow height gain/loss for El Niño and La Niña that are quite different. Snow accumulation tends to start earlier during El Niño periods but results in less overall net accumulation, while during La Niña episodes there is a later onset of the wet season but greater overall snow accumulation. This climate response was particularly pronounced during the 2015–2016 El Niño, when net snow height change decreased. These ENSO variable snow gain/loss observations from the Quelccaya AWS are consistent with previous observations that La Niña corresponds with wetter SASM seasons compared with those of El Niño (Garreaud et al., 2003; Paegle & Mo, 2002). This has been generally attributed to modulation of the tropical zonal overturning Walker Circulation (Grimm, 2003, 2004).

2.3.4. Temperature

Average global surface temperatures are warmer during El Niño (Halpert & Ropelewski, 1992). Over tropical South America, ENSO variability is also characterized by warmer temperatures during El Niño (Figures 3c and 7). The response of surface temperature to tropical SSTs is more pronounced over the northeastern Amazon Basin, compared with that over the western Atlantic Ocean or the western Amazon Basin. During El Niño, austral summers and winters over the western Amazon and Quelccaya are warmer and colder, respectively (Figure 8a). Over the western Amazon Basin and the vicinity of Quelccaya, temperature seasonality is amplified during El Niño and reduced during La Niña (Figure 8b). The enhanced temperature seasonality during El Niño is particularly pronounced in late summer (March-April) and winter (August-September) when both snowfall amount and variability is relatively low. The impact that ENSO temperature variability has on the Rayleigh fractionation models is shown in Figures 8c and 8d and the zoom inset plot. Figure 8c is

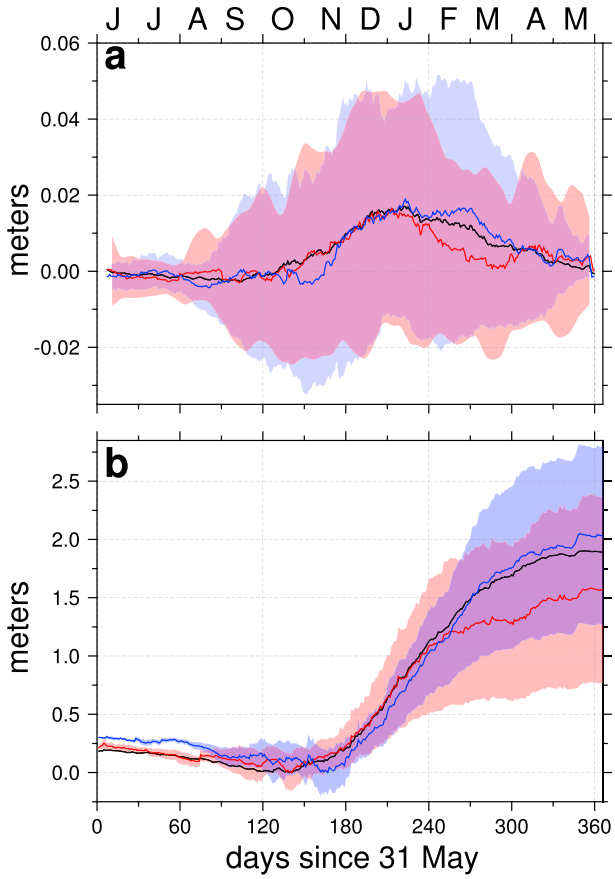

Figure 6. (a) Observed Quelccaya daily snow height change for the hydrologic year (June-May). Solid curves and shading are the mean and the mean ±1 standard deviation for all data (black, no shading), red = El Nino, and blue = La Nina. (b) Observed Quelccaya cumulative snow height change for the hydrologic year (June-May). Cumulative values are referenced to the yearly minimum cumulative snow height (*y* axis). Black = 2003–2017 long-term mean, red = El Niño, and blue = La Niña. *X* axis is day of the hydrologic year or days since 31 May; 1 June = day 1.

the traditional Rayleigh model perspective in q versus δD space, and isotope ratios are plotted against temperature in Figure 8d to illustrate the role of temperature. Warmer austral summer temperatures, and as a consequence higher q, during El Niño displace the Rayleigh curves to the right on the q or x axis, or below the La Niña curve on the hydrogen isotope ratio axis (y axis). The vertical offset in values between the red and blue curves in Figure 8d (for δD) corresponds to a change in snow δ^{18}O of <1‰.

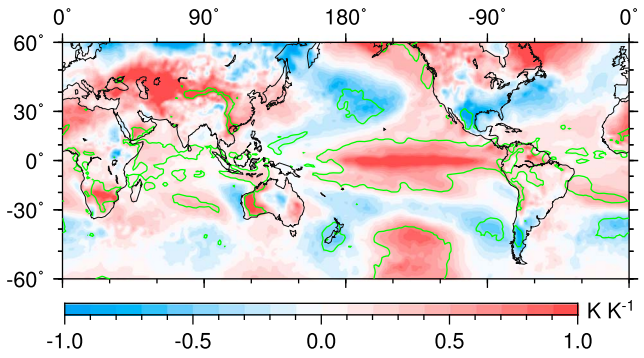

Figure 7. Linear regression coefficient between the Oceanic Niño Index (ONI, monthly SST anomalies) and surface temperature (ERA-Interim, 2003–2017). Green lines encompass areas where the correlation between ONI and surface temperature is significant at the 95% confidence level.

2.3.5. Initial Vapor Isotope Ratios

As a consequence of ENSO affecting upstream convection in the SASM domain (Vuille & Werner, 2005), initial vapor isotope ratios vary according to ENSO phase. The SASM is more active during La Niña, which yields lower water vapor δ values downstream in the lower troposphere over the western Amazon Basin (Figure 9).

In practice, and in the Rayleigh models used for the PSM, the isotope ratio of the initial water vapor is taken as the δ value from the lower troposphere over the western Amazon Basin, as this is the air that feeds into convection up to an altitude above Quelccaya. The isotope ratio of this lower troposphere western Amazon Basin water vapor is effectively a product of upstream convection. Moisture is transported by low-level easterlies from the tropical Atlantic across the Amazon Basin. There is a higher amplitude seasonality of lower troposphere water vapor isotope ratios over the western Amazon Basin, compared with the tropical Atlantic (Hurley et al., 2016). This is due to intense convective activity

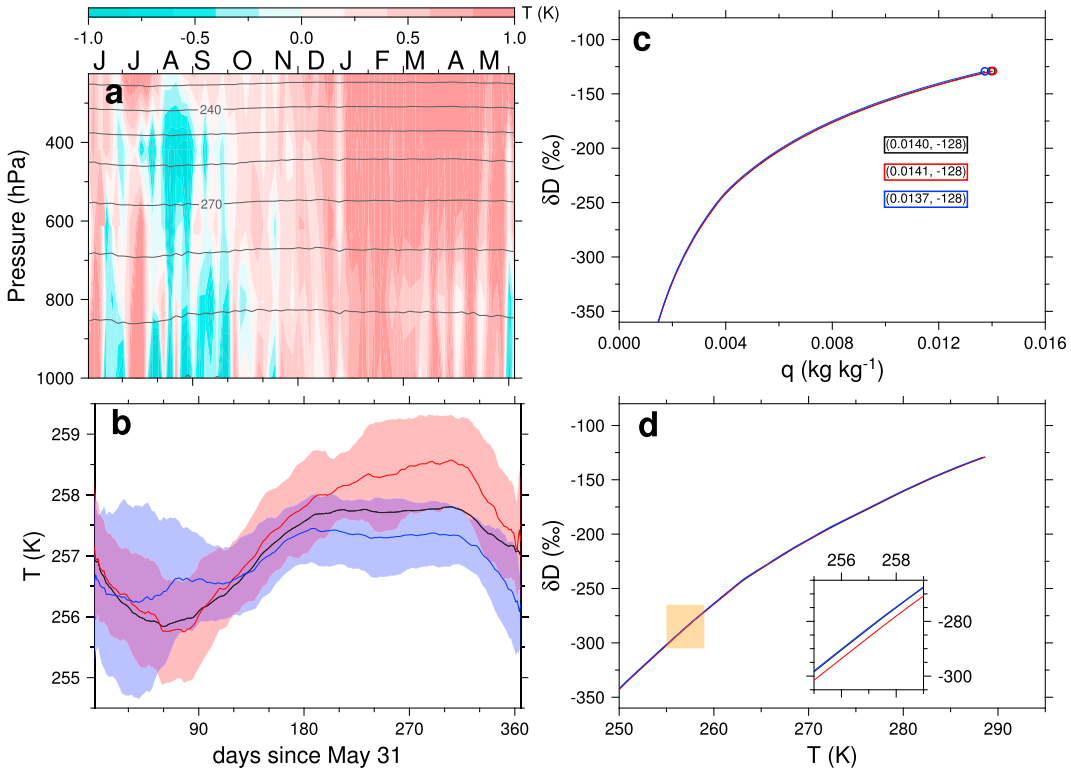

Figure 8. Western Amazon Basin and Quelccaya temperature seasonality. (a) Seasonality of the vertical temperature structure. El Niño minus La Niña temperature over the western Amazon Basin (color shading) with the climatological mean as gray contours. The western Amazon Basin is defined as 67°W–73°W, 7°S to 13°S. (b) Seasonality of 400-hPa temperature over Quelccaya; black = mean, red = El Niño, and blue = La Niña. Solid curves are mean values and shading is mean ±1 standard deviation. (c) Example Rayleigh model curves for 1 January of water concentration, q, versus δD for the Q-CTRL (black), El-ΔT (red), and La-ΔT (blue) simulations. Water vapor initial conditions for q and δD are indicated by open circles, and values are listed in color-coded boxes. (d) Example T versus δD curves from 1 January Rayleigh models used in the Q-CTRL (black), El-ΔT (red), and La-ΔT (blue) simulations. The inset highlights the El Niño–Southern Oscillation variability in temperature conditions over Quelccaya (400 hPa, beige-shaded box).

along the air mass trajectory over the Amazon Basin during austral summer, effectively depleting the remaining water vapor in heavy isotopes once it reaches the westernmost part of the basin.

3. Results

Comparing the results of the ENSO-phase sensitivity simulations with both the observations and the control simulations (Figure 10a) shows that the ENSO-induced variability in δ^{18}O is best accounted for by changes to the initial water vapor delta value, $\delta_{v,i}$. The response of the PSM to ENSO-related changes in both local snow gain/loss, Δh_s, and temperature, ΔT, are much smaller in amplitude. The ENSO-related temperature effect by itself yields a response that is opposite in sign from the observed ENSO variability.

The simulated responses of Quelccaya δ^{18}O to ENSO-induced changes in the local snow gain/loss are of the same sign as the observations, but the amplitude of the observed change is underestimated by the simulations (Figure 10a, Δh_s). By altering the timing of snowfall events throughout the hydrologic year, local snow gain/loss does impact the archive of δ^{18}O at Quelccaya. An early demise of the summer monsoon with reduced snowfall in the second half of the wet season (February-April, El Niño red curve in Figure 6a) appears to contribute to the observed signal by reducing snow accumulation during the latter parts of the summer when isotope ratios are the most negative.

When we isolate the influence of ENSO-related air temperature changes, and consequent changes in q, on Quelccaya δ^{18}O, the sign of the simulated response is opposite that of the observations and smaller in amplitude (Figure 10a, ΔT). This is a direct result of warmer Rayleigh fractionation during El Niño

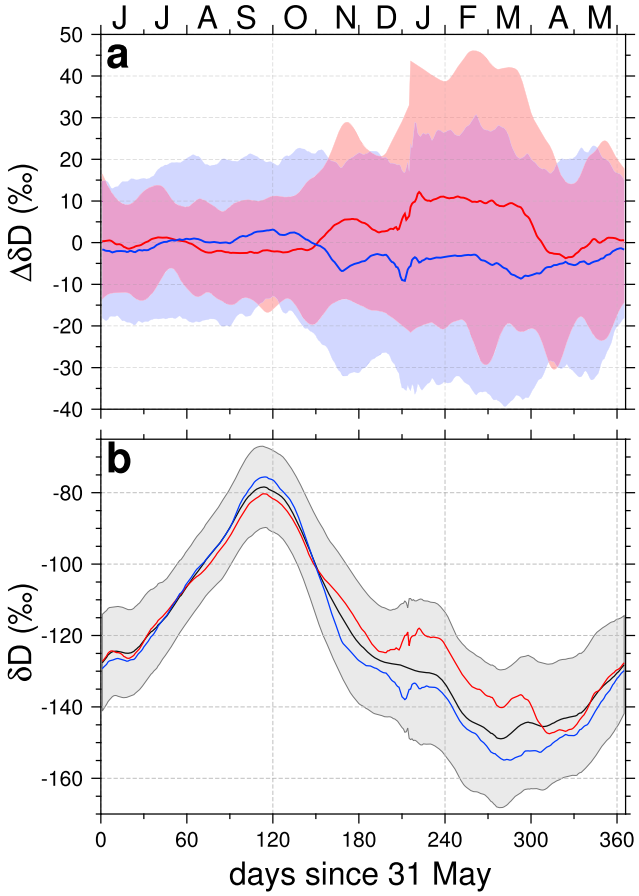

Figure 9. (a) ENSO-phase anomalies of western Amazon Basin water vapor δD (IsoGSM) in the lower troposphere. The western Amazon Basin is defined as 67°W–73°W, 7°S to 13°S. Solid curves and shading are mean and mean ±1 standard deviation for El Niño (red) and La Niña (blue). (b) Seasonality of western Amazon Basin water vapor δD for the lower troposphere, black solid curve and shading are TES mean seasonal cycle and red and blue are TES mean plus the IsoGSM El Niño and La Niña seasonal cycle anomalies, respectively. These values constrain the Rayleigh curve initial vapor δ values.

(red versus blue curve in Figures 8c and 8d). This is distinct from a colder final fractionation temperature along a common Rayleigh curve, which will yield a lower isotope ratio.

When the PSM is forced by ENSO-induced changes to the lower tropospheric water vapor δ values over the western Amazon Basin, the simulated ENSO response of Quelccaya δ^{18}O matches the observations in both sign and amplitude (Figure 10a, $\Delta\delta_{v,i}$). This result reaffirms the importance of the properties of the initial water vapor in constraining the precipitation isotope ratio and ties the Quelccaya ice core isotopic record to the strength of the hydrologic cycle upstream and to the large-scale atmospheric dynamics of the SASM region.

In Figure 10b we recast the results shown in Figure 10a as departures from the Q-CTRL simulation to focus exclusively on the model response. The ENSO responses of the model simulated by El-CTRL and La-CTRL are dominated by the initial vapor δ value forcing. The impact that Δh_s and T have on the simulated δ^{18}O is less than half that of $\delta_{v,i}$. On interannual time scales $\delta_{v,i}$ varies primarily in response to SASM activity. The results of the ENSO-phase sensitivity simulations suggest that ENSO variability of Quelccaya δ^{18}O is primarily a response, for example, during La Niña, of enhanced rainout over the Amazon Basin, consequent lowering of water vapor δ values over the western Amazon Basin, and Rayleigh fractionation of vapor with lower $\delta_{v,i}$. This physically ties interannual variability of tropical Pacific SSTs to isotope ratios in tropical Andean snow and ice in ways that are not strictly temperature related.

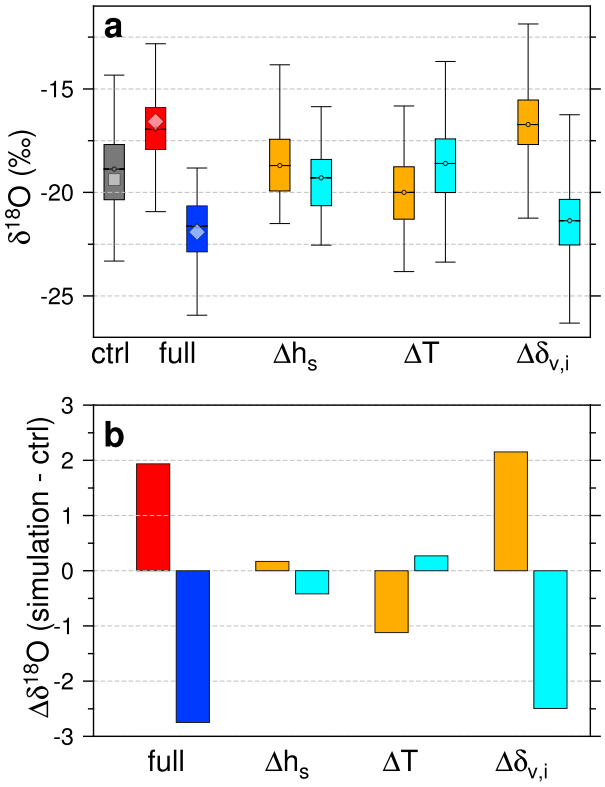

Figure 10. (a) Observed (small gray square and red and blue diamonds) and simulated Quelccaya snow δ^{18}O values according to ENSO phase. Gray = Q-CTRL, red = El-CTRL, blue = La-CTRL, orange = El Niño phase sensitivity simulations and cyan = La Niña simulations for local snow gain/loss (Δh_s), temperature (ΔT), and water vapor initial isotope ratio ($\Delta\delta_{v,i}$). (b) Simulated Quelccaya snow δ^{18}O expressed as departures from the Q-CTRL simulation mean isotope ratio. Red = El-CTRL, blue = La-CTRL, orange = El Niño phase sensitivity simulations and cyan -La Niña simulations for Δh_s, ΔT, and $\Delta\delta_{v,i}$ ENSO-phase simulation.

Isotope ratios are generally and inherently a function of temperature owing to the temperature dependence of the fractionation factor. For instance, the "temperature effect" describes observed patterns of lower water vapor isotope ratios at higher latitudes, in concert with temperature (Dansgaard, 1964). Water vapor stable isotope ratios are however also a consequence of the conditions (temperature and pressure) at which the air had last encountered saturation and condensation (Galewsky & Hurley, 2010). The dependence of lower troposphere water vapor isotope ratios over the western Amazon Basin on both (i) upstream precipitation and (ii) subsequent transport, helps to tie Quelccaya snow isotope ratios to the hydrologic cycle and the large-scale circulation.

4. Discussion and Conclusions

During El Niño, there is less snow accumulation at Quelccaya; austral summer precipitation has an earlier onset than it does during La Niña, and there is less middle to late summer snowfall. There is an amplification of the Quelccaya and western Amazon Basin seasonal temperature cycle during El Niño: higher temperature during austral summer and lower temperature during austral winter. There is a weakening of the SASM over the Amazon Basin during El Niño in a manner consistent with weakened upper troposphere tropical easterlies. The weakened hydrologic cycle during austral summer reduces rainout upstream over the central Amazon, thereby resulting in higher overall δ^{18}O at Quelccaya. This is not unlike the explanation for seasonality of δ^{18}O put forth by Grootes et al. (1989) and more recently described in our development of a tropical Andean ice core PSM (Hurley et al., 2016). Here we used the PSM developed in that study for completing a series of ENSO-phase sensitivity simulations to distinguish the relative roles of the local snow gain/loss, temperature, and the water vapor initial δ value in forcing the ENSO signal of tropical Andean δ^{18}O.

We find that most of the ENSO variability in Quelccaya δ^{18}O can be explained by changes in SASM activity and its influence on downstream water vapor δ values that feed into Rayleigh fractionation, from the lower troposphere over the western Amazon Basin up to the altitude of snow formation over the ice cap. The large-scale circulation also plays a key role in the transport of vapor to the western Amazon Basin.

There are also changes to the low-level circulation in response to ENSO (Figure 3d). The northerly low-level jet that exports tropical heat and energy to higher latitudes is weaker during La Niña. Most of this poleward heat transport east of the Andes is associated with cold air incursion activity (Garreaud, 2001). Cold air incursions begin as extratropical high-pressure systems. As they advance northward, convection occurs along their equatorward fronts (Garreaud, 1999, 2000). They traverse from southern South America into the western Amazon Basin, and we have previously identified them as responsible for most of the snowfall at Quelccaya (Hurley et al., 2015). ENSO variability of cold air incursions is not well characterized, particularly as it pertains to hydroclimate of the western Amazon Basin or the tropical Andes. Perhaps northerly low-level jet ENSO variability is a consequence of cold air incursion activity; that is, more active cold air incursions during La Niña would weaken the northerly low-level jet and account for changes in the water vapor isotope ratios over the western Amazon Basin. Here we attribute the ENSO variability in western Amazon Basin lower troposphere water vapor isotope ratios to upstream precipitation associated with the SASM (which does include western Amazon Basin cold air incursion precipitation). It is possible that there are nuances of this interpretation that could be attributed to the large-scale circulation changes via modulation of cold air incursion activity, and we leave this for future work. The PSM used in this study is limited in that it does not account for circulation changes. However, given the dynamical conditions presented in Figures 3c and 3d, most of the moisture that undergoes convection along the fronts of cold air incursions are likely from the north and east, evaporated from the Atlantic and transported or recycled over the Amazon Basin.

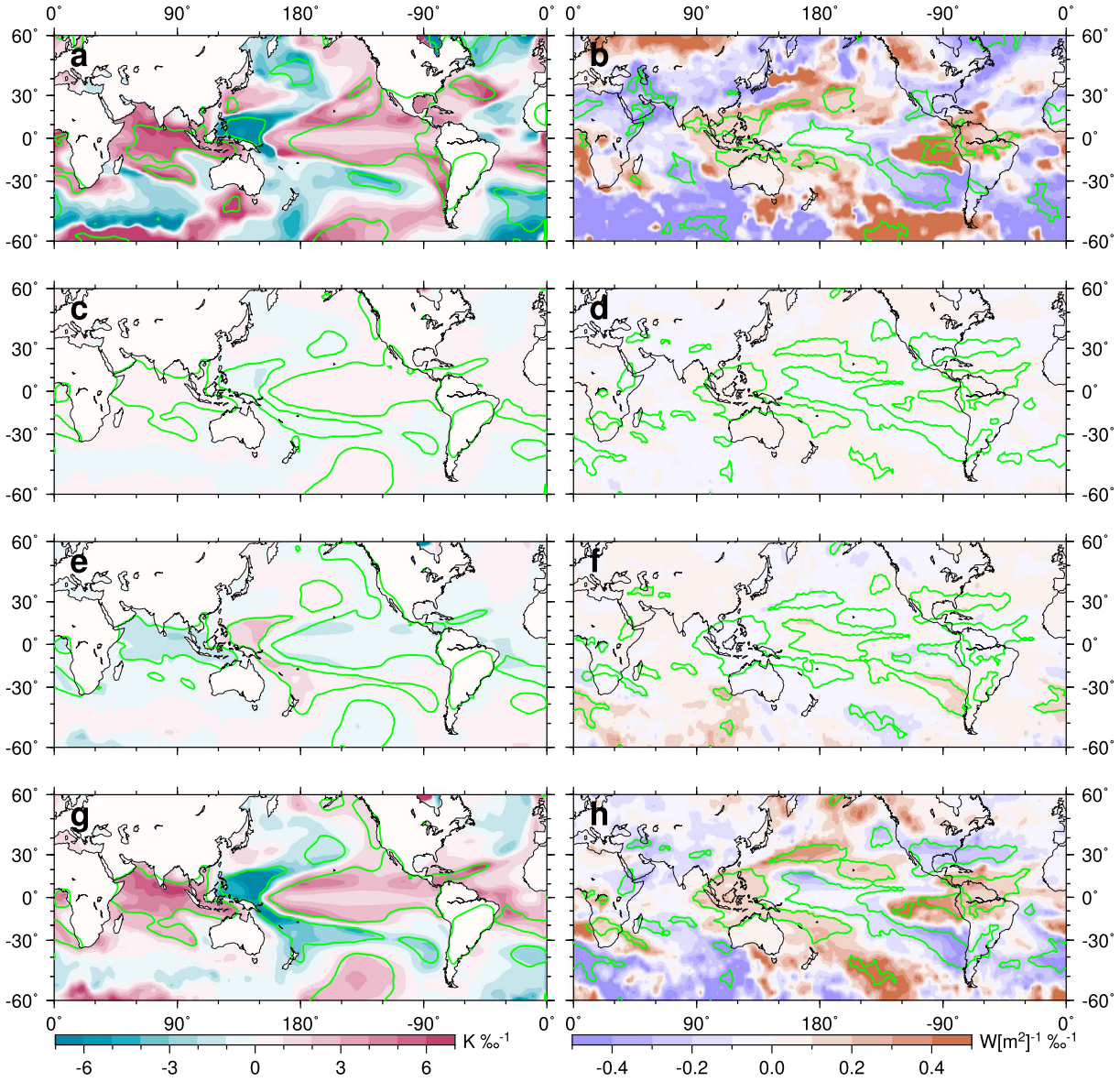

Figure 11. Austral summer (DJF) SST (left column) and OLR (right column) regressed against (a, b) observed QIC δ^{18}O, (c, d) QIC δ^{18}O from the local snow gain/loss simulations, (e, f) QIC δ^{18}O from the temperature simulations, and (g, h) QIC δ^{18}O from the water vapor initial δ value simulations. Green lines surround areas where the correlation between QIC δ^{18}O and SST or OLR is significant at the 95% confidence level.

Limitations to this study also include a lack of observational constraints on details of the Rayleigh fractionation models. For instance, the altitude of condensation above Quelccaya is assumed to be the pressure level (400 hPa) above the summit. This parameter likely varies throughout the year and on synoptic time scales. The time period of our study, about 14 years, also presents a limitation particularly on the application of our results to multidecadal variability from the Quelccaya paleoclimate archive for the last 1,800 years.

The results presented here do highlight the importance of the initial water vapor isotope ratio as a function of monsoon dynamics and clarify that the isotope signal should not be interpreted as a simple temperature response. Furthermore, we see from our results that the seasonality of the local hydrologic cycle and the seasonal distribution of snowfall events also has an influence on the isotope archive. In the examples shown here, enhanced late summer snowfall during La Niña helps to preserve more negative isotope ratios at Quelccaya, because water vapor isotope ratios in the lower troposphere over the western Amazon Basin reach their minimum at this time. However, this impact is relatively small compared with the influence of the initial water vapor isotope ratio.

To further consider the interannual relationships between Quelccaya isotope ratios, ENSO, and the monsoon, we completed field correlation and regression analyses (Figure 11) between the observed and simulated Quelccaya $\delta^{18}O$ archives and both SST and OLR. Regression of observed Quelccaya $\delta^{18}O$ with SSTs exhibits typical ENSO patterns (Figure 11a), as would be expected. Warmer SSTs in the eastern tropical Pacific such as during El Niño correspond with higher $\delta^{18}O$ ratios at Quelccaya. Regression of observed Quelccaya $\delta^{18}O$ with OLR also exhibits expected and ENSO-like patterns (Figure 11b). Anomalous convective activity (low OLR) over the Amazon Basin (such as occurs during La Niña) corresponds with lower $\delta^{18}O$ ratios at Quelccaya. We then completed the same field correlation and regression analyses against SST and OLR, using the simulated Quelccaya $\delta^{18}O$ archives. These analyses were completed by correlating and regressing SST and OLR against the simulated $\delta^{18}O$ archives that were computed using the PSM forced with isolated ENSO variability of (i) local snow gain/loss (Figures 11c and 11d), (ii) temperature (Figures 11e and 11f), and (iii) the water vapor initial δ value (Figures 11g and 11h). As we showed in the previous section for the annual time series, the spatial patterns of the slope of the linear relationship between Quelccaya $\delta^{18}O$ and both local snow gain/loss (Figures 11c and 11d) and temperature (Figures 11e and 11f) are weak, compared with the observed relationships. We find that most of the observed linear spatial patterns between $\delta^{18}O$ and both SST and OLR are accounted for by variability in the initial water vapor δ-value over the western Amazon Basin (Figures 11g an 11h). Importantly, these patterns are consistent with ENSO climate variability and demonstrate the connections between tropical Pacific SST, convection over the Amazon Basin, and Quelccaya $\delta^{18}O$. The positive relationship between observed Quelccaya $\delta^{18}O$ and Amazon Basin OLR reflects upstream convection and rainout, thereby lowering water vapor δ values that then impact downstream precipitation over the Andes. Similar mechanisms have been observed in Tibet, where precipitation isotope ratios have been correlated with upstream convection over India (He et al., 2015), and from both the western Africa (Okazaki et al., 2015) and Asian (Ishizaki et al., 2012) monsoon regions.

It is important to consider how the results of our study may have bearing on the interpretation of the 1,800-year Quelccaya $\delta^{18}O$ archive. For example, Rojas et al. (2016) recently presented modeling results that suggest the SASM was strengthened during the Little Ice Age (LIA, 1450-1850 CE) compared with the Medieval Climate Anomaly (MCA, 950-1250 CE). Quelccaya isotope ratios were indeed lower during the LIA, consistent with our results presented here. A number of additional archives in the tropical Andes, which also incorporate the isotopic composition of Andean precipitation and hence western Amazon Basin water vapor into their record, show similar negative departures in their isotopic signal during the LIA (e.g. Apaestegui et al., 2014; Bird et al., 2011; Kanner et al., 2013; Vuille et al., 2012). Conversely, the MCA may have represented a period of reduced monsoon intensity which led to higher water isotopologue ratios over the western Amazon Basin and at Quelccaya. Our results show that the past joint history of ENSO and SASM are tied to Quelccaya $\delta^{18}O$, and call for re-interpretation of the QIC isotope archive, particularly as it relates to convection and water vapor isotope histories over the Amazon Basin. Turning to the future, extreme El Niño events give rise to catastrophic weather phenomena and they are expected to become more frequent as a function of global warming (Santoso et al., 2013). In that regard, we expect that the results presented here may provide some guidance in interpretating how global-warming influences South American and Andean hydrology.

Acknowledgments
The authors thank three reviewers whose comments vastly improved the quality of this paper. ERA-Interim reanalysis was obtained from the Research Data Archive (RDA) that is maintained by the Computational and Information Systems Laboratory at the National Center for Atmospheric Research (NCAR). NCAR is sponsored by the National Science Foundation (NSF). The original data are available from the RDA (http://rda.ucar.edu) in data set ds627.0. GPCP 1° daily precipitation data were obtained from the NASA Goddard Space Flight Center (http://precip.gsfc.nasa.gov). TES Lite Products data were obtained from the NASA Jet Propulsion Laboratory (tes. jpl.nasa.gov/data/). The authors gratefully acknowledge the financial support from NSF-P2C2 (AGS-1303828, AGS-1702789), NSF Paleoclimate (9909201 and 0402557), and the NOAA Global Climate Observing System. NOAA Extended Reconstructed Sea Surface Temperature (ERSST) version 5 was obtained from DOC/NOAA/NESDIS/NCEI National Centers for Environmental Information, doi:10.7289/V5T72FNM. Interpolated OLR data were obtained from the NOAA/OAR/ESRL PSD, Boulder, Colorado (https://www.esrl.noaa.gov/psd/). IsoGSM water vapor isotope data were obtained from Kei Yoshimura. Data unique to this study are included in the supporting information of this paper.

References

Apaestegui, J., Cruz, F. W., Sifeddine, A., Vuille, M., Espinoza, J. C., Guyot, J. L., et al. (2014). Hydroclimate variability of the northwestern Amazon Basin near the Andean foothills of Peru related to the South American Monsoon System during the last 1600 years. *Climate Past*, *10*, 1967–1981. https://doi.org/10.5194/cp-10-1967-2014

Barnard, P. L., Hoover, D., Hubbard, D. M., Snyder, A., Ludka, B. C., Allan, J., et al. (2017). Extreme oceanographic forcing and coastal response due to the 2015–16 El Niño. *Nature Communications*, *8*, 14365. https://doi.org/10.1038/ncomms14365

Bird, B. W., Abbott, M. B., Vuille, M., Rodbell, D. T., Stansell, N. D., & Rosenmeier, M. F. (2011). A 2,300-year-long annually resolved record of the South American summer monsoon from the Peruvian Andes. *PNAS*, *108*(21), 8583–8588. https://doi.org/10.1073/pnas.1003719108

Bradley, R. S., Keimig, F. T., & Diaz, H. F. (2004). Projected temperature changes along the American cordillera and the planned GCOS network. *Geophysical Research Letters*, *31*, L16210. https://doi.org/10.1029/2004/GL020229

Bradley, R. S., Keimig, F. T., Diaz, H. F., & Hardy, D. R. (2009). Recent changes in freezing level heights in the Tropics with implications for the deglaciation of high mountain ranges. *Geophysical Research Letters*, *36*, L17701. https://doi.org/10.1029/2009GL037712

Bradley, R. S., Vuille, M., Hardy, D. R., & Thompson, L. G. (2003). Low latitude ice cores record Pacific sea surface temperatures. *Geophysical Research Letters*, *30*(4), 1174. https://doi.org/10.1029/2002GL016546

Climate Prediction Center (2018). National Centers Environmental Prediction, NOAA, origin.cpc.ncep.noaa.gov/products/analysis_monitoring/ensostuff/ONI_v5.php.

Craig, H. (1961). Isotopic variations in meteoric waters. *Science*, *133*(3465), 1702–1703. https://doi.org/10.1126/science.133.3465.1702

Dansgaard, W. (1964). Stable isotope in precipitation. *Tellus*, *16*, 436–468.
Dee, D. P., Uppala, S. M., Simmons, A. J., Berrisford, P., Poli, P., Kobayashi, S., et al. (2011). The ERA-Interim reanalysis: configuration and performance of the data assimilation system. *Quarterly Journal of the Royal Meteorological Society*, *137*, 553–597.
Evans, M. N., Tolwinski-Ward, S. E., Thompson, D. M., & Anchukaitis, K. J. (2013). Applications of proxy system modeling in high resolution paleoclimatology. *Quaternary Science Reviews*, *76*, 16–28. https://doi.org/10.1016/j.quascirev.2013.05.024
Francou, B., Vuille, M., Favier, V., & Cáceres, B. (2004). New evidence for an ENSO impact on low-latitude glaciers: Antizana 15, Andes of Ecuador, 0°28′S. *Journal of Geophysical Research*, *109*(D18), D18106. https://doi.org/10.1029/2003JD04484
Francou, B, Vuille, M., Wagnon, P., Mendoza, J., & Sicart, J.-E. (2003). Tropical climate change recorded by a glacier in the central Andes during the last decades of the twentieth century: Chacaltaya, Bolivia, 16°S. *Journal of Geophysical Research*, *108*(D5), 4154. https://doi.org/10.1029/2002JD002959
Galewsky, J., & Hurley, J. V. (2010). An advection-condensation model for subtropical water vapor isotopic ratios. *Journal of Geophysical Research*, *115*, D16116. https://doi.org/10.1029/2009JD013651
Garreaud, R. (1999). Cold air incursions over subtropical and tropical South America: A numerical case study. *Monthly Weather Review*, *127*, 2823–2853. https://doi.org/10.1175/1520-0493(1999)127<2823:CAIOSA>2.0.CO;2
Garreaud, R. (2000). Cold air incursions over subtropical and tropical South America: Mean structure and dynamics. *Monthly Weather Review*, *128*, 2544–2559. https://doi.org/10.1175/1520-0493(2000)128<2544:CAIOSS>2.0.CO;2
Garreaud, R. D. (2001). Subtropical cold surges: Regional aspects and global distribution. *International Journal of Climatology*, *21*, 1181–1197. https://doi.org/10.1002/joc.687
Garreaud, R., Vuille, M., & Clement, A. (2003). The climate of the Altiplano: Observed current conditions and mechanisms of past changes. *Palaeogeography, Palaeoclimatology, Palaeoecology*, *194*, 5–22. https://doi.org/10.1016/S0031-0182(03)00269-4
Grimm, A. M. (2003). The El Niño impact on the summer monsoon in Brazil: Regional processes versus remote influences. *Journal Climate*, *16*, 263–280. https://doi.org/10.1175/1520-0442(2003)016<0263:TENIOT>2.0.CO;2
Grimm, A. M. (2004). How do La Niña events disturb the summer monsoon system in Brazil? *Climate Dynamics*, *22*, 123–138. https://doi.org/10.1007/s00382-003-0368-7
Grootes, P. M., Stuiver, M., Thompson, L. G., & Mosley-Thompson, E. (1989). Oxygen isotope changes in tropical ice, Quelccaya, Peru. *Journal of Geophysical Research*, *94*(D1), 1187–1194.
Halpert, M. S., & Ropelewski, C. F. (1992). Surface temperature patterns associated with the Southern Oscillation. *Journal Climate*, *5*, 577–593. https://doi.org/10.1175/1520-0442(1992)005<0577:STPAWT>2.0CO;2
He, Y., Risi, C., Gao, J., Masson-Delmotte, V., Yao, T., Lai, C.-T., et al. (2015). Impact of atmospheric convection on south Tibet summer precipitation isotopologue composition using a combination of in situ measurements, satellite data, and atmospheric general circulation modeling. *Journal of Geophysical Research: Atmospheres*, *120*, 3852–3871. https://doi.org/10.1002/2014JD022180
Huang, B., L'Heureux, M., Hu, Z.-Z., & Zhang, H.-M. (2015). Ranking the strongest ENSO events while incorporating SST uncertainty. *Geophysical Research Letters*, *43*, 9165–9172. https://doi.org/10.1002/2016GL070888
Huang, B., Thorne, P. W., Banzon, V. F., Boyer, T., Chepurin, G., Lawrimore, J. H., et al. (2017). Extended reconstructed sea surface temperature, Version 5 (ERSSTv5): Upgrades, Validations, and Intercomparisons. *Journal of Climate*, *30*, 8179–8205. https://doi.org/10.1175/JCLI-D-16-0836.1
Hurley, J. V., Vuille, M., & Hardy, D. R. (2016). Forward modeling of δ^{18}O in Andean ice cores. *Geophysical Research Letters*, *43*, 7467–7487. https://doi.org/10.1002/2016GL070150
Hurley, J. V., Vuille, M., Hardy, D. R., Burns, S. J., & Thompson, L. G. (2015). Cold air incursions, δ^{18}O variability, and monsoon dynamics associated with snow days at Quelccaya Ice Cap, Peru. *Journal of Geophysical Research: Atmospheres*, *120*, 8178–8188. https://doi.org/10.1002/2016GL070150
Ishizaki, Y, Yoshimura, K., Kanae, S., Kimoto, M., Kurita, N., & Oki, T. (2012). Interannual variability of $H_2^{18}O$ in precipitation over the Asian monsoon region. *Journal of Geophysical Research*, *117*, D16308. https://doi.org/10.1029/2011JD015890
Jiménez-Muñoz, J. C., Mattar, C., Barichivich, J., Santamaría-Artigas, A., Takahashi, K, Malhi, Y., et al. (2016). Record-breaking warming and extreme drought in the Amazon rainforest during the course of El Niñ,o 2015-2016. *Scientific Reports*, *98*(7), 1363–1382. https://doi.org/10.1038/srep33130
Kanner, L. C., Burns, S. J., Cheng, H., Edwards, R. L., & Vuille, M. (2013). High-resolution variability of the South American summer monsoon over the last seven millennia: Insights from a speleothem record from the central Peruvian Andes. *Quaternary Science Reviews*, *75*, 1–10. https://doi.org/10.1016/j.quascirev.2013.05.008
Krishnamurthy, V., & Misra, V. (2010). Observed ENSO teleconnections with the South American monsoon system. *Atmospheric Science Letters*, *11*, 7–12. https://doi.org/10.1002/asl.245
L'Heureux, M. L., Takahashi, K., Watkins, A. B., Barnston, A. G., Becker, E. J., DiLiberto, T. E., et al. (2017). Observing and predicting the 2015-16 El Niñ,o. *Bulletin of the American Meteorological Society*, *98*(7), 1363–1382. https://doi.org/10.1175/BAMS-D-16-0009.1
Lee, H.-T. (2014). Climate algorithm theoretical basis document (C-ATBD): Outgoing longwave radiation (OLR)-Daily. NOAA's climate data record (CDR) program, CDRP-ATBD-0526, 46 pp.
National Aeronautics and Space Administration (2015). Jet Propulsion Laboratory, Aura TES Group, TES Lite Products, [Available at http://avdc.gsfc.nasa.gov].
Okazaki, A., Satoh, Y., Tremoy, G., Vimeux, F., Scheepmaker, R., & Yoshimura, K. (2015). Interannual variability of isotopic composition in water vapor over western Africa and its relationship to ENSO. *Atmospheric Chemistry and Physics*, *15*, 3193–3204. https://doi.org/10.5194/acp-15-3193-2015
Paegle, J. N., & Mo, K.-C. (2002). Linkages between summer rainfall variability over South America and sea surface temperature anomalies. *Journal Climate*, *15*, 1389–1407. https://doi.org/10.1175/1520-0442(2002)015<1389:LBSRVO>2.0.CO;2
Rabatel, A., Francou, B., Soruco, A., Gomez, J., Cáceres, B., Ceballos, J. L., et al. (2013). Current state of glaciers in the tropical Andes: A multi-century perspective on glacier evolution and climate change. *The Cryosphere*, *7*, 81–102. https://doi.org/10.5194/tc-7-81-2013
Rojas, M., Arias, P. A., Flores-Aqueveque, V., Seth, A., & Vuille, M. (2016). The South American monsoon variability over the last millennium in climate models. *Climate Past*, *12*, 1681–1691. https://doi.org/10.5194/cp-12-1681-2016
Samuels-Crow, K., Galewsky, J., Hardy, D. R., Sharp, Z. D., Worden, J., & Braun, C. (2014). Upwind convective influences on the isotopic composition of atmospheric water vapor over the tropical Andes. *Journal of Geophysical Research: Atmospheres*, *119*, 7051–7063. https://doi.org/10.1002/2014JD021487
Santoso, A., McGregor, S., Jin, F.-F., Cai, W., England, M. H., An, S.-I., et al. (2013). Late-twentieth-century emergence of the El Niño propagation asymmetry and future projections. *Nature*, *504*, 126–130. https://doi.org/10.1038/nature12683
Santoso, A., McPhaden, M. J., & Cai, W. (2017). The defining characteristics of ENSO extremes and the strong 2015/2016 El Niño. *Review of Geophysics*, *55*, 1079–1129. https://doi.org/10.1002/2017RG000560

Thompson, L. G., Davis, M. E., Mosley-Thompson, E., Beaudon, E., Porter, S. E., Kutuzov, S., et al. (2017). Impacts of recent warming and the 2015/16 El Niño on tropical Peruvian ice fields. *Journal of Geophysical Research: Atmospheres*, *122*, 12,688–12,701 https://doi.org/10.1002/2017JD026592

Thompson, L. G., Mosley-Thompson, E., Davis, M. E., Zagarodnov, V. S., Howat, I. M., Mikhalenko, V. N., & Lin, P. N. (2013). Annually resolved ice core records of tropical climate variability over the past 1800 years. *Science*, *340*, 945–950.

Vimeux, F., Ginot, P., Schwikowski, M., Vuille, M., Hoffman, G., Thompson, L. G., & Schotterer, U. (2009). Climate variability during the last 1000 years inferred from Andean ice cores: A review of methodology and recent results. *Palaeogeography, Palaeoclimatology, Palaeoecology*, *281*, 229–241.

Vuille, M., Bradley, R. S., Healy, R., Werner, M., Hardy, D. R., Thompson, L. G., & Keimig, F. (2003b). Modeling δ^{18}O in precipitation over the tropical Americas: 2. Simulation of the stable isotope signal in Andean ice cores. *Journal of Geophysical Research*, *108*(D6), 4175.

Vuille, M., Bradley, R. S., Werner, M., Healy, R., & Keimig, F. (2003a). Modeling δ^{18}O in precipitation over the tropical Americas: 1. Interannual variability and climatic controls. *Journal of Geophysical Research*, *108*(D6), 4174.

Vuille, M., Burns, S. J., Taylor, B. L., Cruz, F. W., Bird, B. W., Abbott, M. B., et al. (2012). A review of the South American monsoon history as recorded in stable isotopic proxies over the past two millennia. *Climate Past*, *8*, 1309–1321. https://doi.org/10.5194/cp-8-1309-2012

Vuille, M., Francou, B., Wagnon, P., Juen, I., Kaser, G., Mark, B. G., & Bradley, R. S. (2008). Climate change and tropical Andean glaciers: Past, present and future. *Earth-Science Reviews*, *89*, 79–86. https://doi.org/10.1016/j.earscirev.2008.04.002

Vuille, M., & Werner, M. (2005). Stable isotopes in precipitation recording South American summer monsoon and ENSO variability: Observations and model results. *Climate Dynamics*, *25*, 401–413.

Worden, J., Kulawik, S., Frankenberg, C., Payne, V., Bowman, K., Cady-Peirara, K., et al. (2012). Profiles of CH_4, HDO, H_2O, and N_2O with improved lower tropospheric vertical resolution from Aura TES radiances. *Atmospheric Measurement Techniques*, *5*, 397–411.

Worden, J., Noone, D., Galewsky, J., Bailey, A., Bowman, K., Brown, D., et al. (2011). Estimate of bias in Aura TES HDO/H_2O profiles from comparison of TES and in situ HDO/H_2O measurements at the Mauna Loa Observatory. *Atmospheric Chemistry and Physics*, *11*, 4491–4503.

Yoshimura, K., Kanamitsu, M., Noone, D., & Oki, T. (2008). Historical isotope simulation using reanalysis atmospheric data. *Journal of Geophysical Research*, *113*(D19108). https://doi.org/10.1029/2008JD010074